Probing the Lipid-Free Structure and Stability of Apolipoprotein A-I by Mutation[†]

Irina N. Gorshkova,*[,‡] Kalliopi Liadaki,[§] Olga Gursky,[||] David Atkinson,[||] and Vassilis I. Zannis[‡]

Section of Molecular Genetics at Whitaker Cardiovascular Institute and Department of Biophysics, Boston University School of Medicine, 715 Albany Street, Boston, Massachusetts 02118, and Department of Biochemistry and Institute of Molecular Biology and Biotechnology, University of Grete, Heraklion, Grete, Greece 71110

Received June 23, 2000; Revised Manuscript Received October 18, 2000

ABSTRACT: To probe the secondary structure of the C-terminus (residues 165−243) of lipid-free human apolipoprotein A-I (apoA-I) and its role in protein stability, recombinant wild-type and seven site-specific mutants have been produced in C127 cells, purified, and studied by circular dichroism and fluorescence spectroscopy. A double substitution (G185P, G186P) increases the protein stability without altering the secondary structure, suggesting that G185 and G186 are located in a loop/disordered region. A triple substitution (L222K, F225K, F229K) leads to a small increase in the α-helical content and stability, indicating that L222, F225, and F229 are not involved in stabilizing hydrophobic core contacts. The C-terminal truncation Δ(209−243) does not change the α-helical content but reduces the protein stability. Truncation of a larger segment, Δ(185−243), does not affect the secondary structure or stability. In contrast, an intermediate truncation, Δ(198−243), leads to a significant reduction in the α-helical content, stability, and unfolding cooperativity. The internal 11-mer deletion Δ(187−197) has no significant effect on the conformation or stability, whereas another internal 11-mer deletion, Δ(165−175), dramatically disrupts and destabilizes the protein conformation, suggesting that the presence of residues 165−175 is crucial for proper apoA-I folding. Overall, the findings suggest the presence of stable helical structure in the C-terminal region 165−243 of lipid-free apoA-I and the involvement of segment 209−243 in stabilizing interactions in the molecule. The effect of the substitution (G185P, G186P) on the exposure of tryptophans located in the N-terminal half suggests an apoA-I tertiary conformation with the C-terminus located close to the N-terminus.

Human apolipoprotein A-I (apoA-I),[1] a 243 amino acid polypeptide, is the major protein of high-density lipoprotein (HDL) that maintains the structural integrity of the lipoprotein particle and plays a vital role in lipoprotein metabolism, reverse cholesterol transport, and protection against the development of atherosclerosis (*1*−*3*). It is believed that the anti-atherogenic role of the protein is mediated through several apoA-I functions. Some of these functions, such as activation of lecithin:cholesterol acyltransferase (LCAT) (*4*) and cholesterol transfer among lipoproteins (*5*), require a lipid-bound state of the protein. Others, such as cubilin-mediated clearance (*6*) or promotion of cholesterol efflux from cells (*7, 8*), may be performed by either lipid-free or lipid-bound apoA-I. The conformation of apoA-I has been shown to play a central role in regulating the functions of this protein (*9*−*15*). Therefore, a detailed understanding of the conformation and stability of apoA-I, in both the lipid-free and lipid-bound states, is necessary for a full understanding of its functions.

The conformation of plasma apoA-I is driven by characteristic 11/22-residue tandem repeats in the primary sequence that are predicted to form amphiphathic α-helices (*9*). Lipid binding increases the α-helical content of apoA-I by 10−30%, dependent on the amount and composition of bound lipids (*10, 13, 16, 17*). Thus, in the course of HDL metabolism, the conformation of apoA-I changes among the lipid-free and a variety of lipid-bound states. These conformational changes may involve folding−unfolding processes of the protein α-helices facilitated by the absence of strong tertiary interactions in the apoA-I molecule in solution (*9, 18, 19*). This conformational plasticity has hampered the X-ray crystallographic analysis of apoA-I. The low-resolution X-ray crystal structure has been determined only for a truncated recombinant form of apoA-I (44−243) (*20*) that is folded in a highly helical conformation (*21*). In the crystal, this mutant forms an almost continuous helical structure with an overall 'horseshoe' shape that has been suggested to mimic the lipid-bound apoA-I conformation (*20*).

Among several secondary structural predictions based on the apoA-I sequence [reviewed in (*22*)], the model of Nolte and Atkinson (*23*) (Figure 1A), derived using statistical and homology-based prediction algorithms and constrained by circular dichroism (CD) data for apoA-I/DMPC recombinant

[†] This work was supported by Grants HL 48739 and PO1HL 26335 from the National Institutes of Health and by Grant BMH4-CT983699.

* To whom correspondence should be addressed at the Department of Biophysics, Boston University School of Medicine, 700 Albany St., W-322, Boston, MA 02118-2526. Fax: (617) 638-4041. Phone: (617) 638-4207. E-mail: igorshko@bu.edu.

[‡] Section of Molecular Genetics, Boston University School of Medicine.

[§] University of Grete.

[||] Department of Biophysics, Boston University School of Medicine.

[1] Abbreviations: apoA-I, apolipoprotein A-I; CD, circular dichroism; DMPC, dimyristoylphosphatidylcholine; GdnHCl, guanidine hydrochloride; HDL, high-density lipoprotein(s); LCAT, lecitin:cholesterol acyltransferase; WMF, wavelength of maximum fluorescence; WT, recombinant wild-type apoA-I.

10.1021/bi0014406 CCC: $19.00
Published on Web 11/28/2000

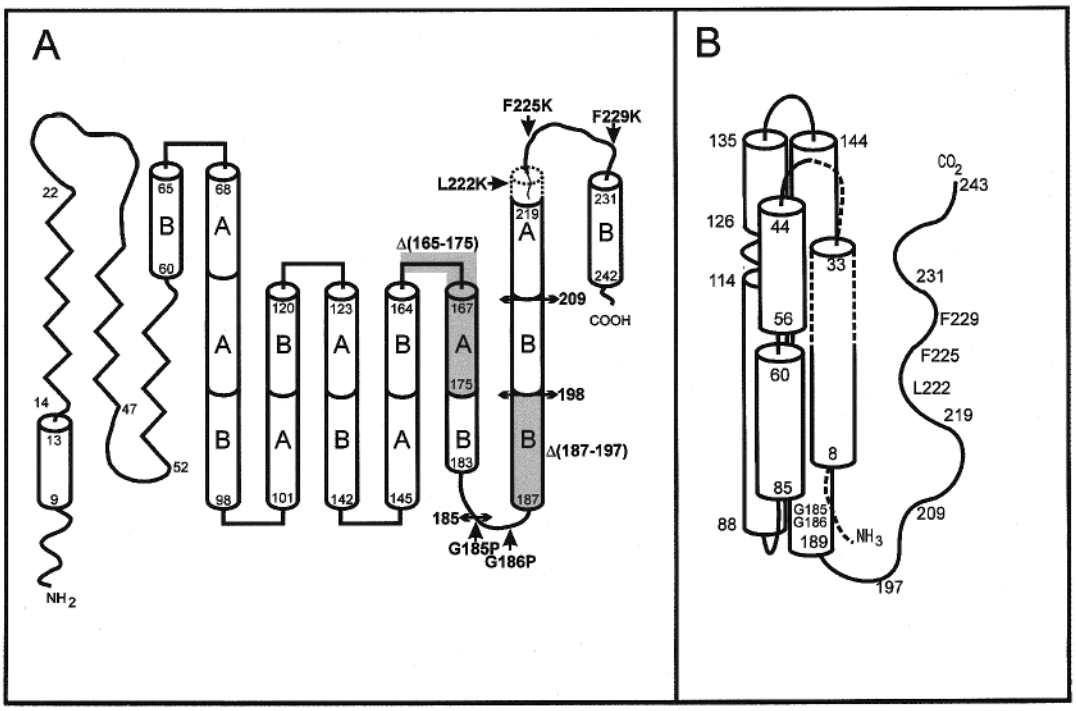

FIGURE 1: Secondary structure models of apoA-I. Cylinders represent helical structures. (A) A prediction made by Notle and Atkinson (*23*) based on the apoA-I sequence and CD data for apoA-I/DMPC recombinant lipoproteins. "A" and "B" in the model indicate, respectively, type "A" and type "B" 11-mer repeats; "A" repeats have most frequently Pro and Ala in positions 1 and 8, respectively; "B" repeats have most frequently Ala and Glu in positions 1 and 8, respectively. The region 220−223 shown by the dotted line and assigned as helical in the model (*23*) has been suggested to be a part of loop/disordered region 220−230, according to our analysis of the (L222K, F225K, F229K) mutation. Sites of mutations analyzed in the work are shown [(→) point mutations, (↔) C-terminal deletions, (shaded cylinders) internal deletions]. (B) A model adapted from Roberts et al. (*24*) that was based on limited proteolysis data of lipid-free apoA-I. Based on subsequent analytical ultracentrifugation data, this helical bundle conformation was proposed to be in dynamic equilibrium with an elongated monomeric helical "hairpin" conformation (*19*).

lipoproteins, contains secondary structure assignments that are in almost exact agreement with the secondary structure determined from the crystal structure of truncated (44−243) apoA-I (*20*). The only exception is the N-terminal segment (44−59) that is helical in the crystal structure of Δ(1−43) apoA-I. However, this two-dimensional model does not predict a tertiary conformation. A four-helix bundle model for lipid-free apoA-I proposed by Roberts et al. (*24*) based on limited proteolysis data (Figure 1B) predicts a disordered C-terminus (residues 190−243) that is thought to become more helical in the lipid-bound state of the protein. This four-helix bundle is proposed to be in dynamic equilibrium with an elongated helical hairpin conformation (*19*). Spectroscopic, thermodynamic, and functional studies of the mutant forms of apoA-I (*5, 11, 12, 19, 21, 25*−*31*) suggest that different portions of the molecule play specific roles in the protein structure, stability, and function. The N-terminus (residues 1−43) is suggested to be an important determinant of the structure and stability of the lipid-free protein (*19, 21, 25*). The region (88−98) is critical for proper folding of both the lipid-free and lipid-bound conformations (*27*). The C-terminal portion of the protein (residues 190−243) affects the rate of lipid binding (*28, 29*). The C-terminal half (residues 139−243) is thought to form additional α-helical structure in the lipid-bound state (*25*). The secondary structure of the C-terminal portion of apoA-I in the lipid-free state and its role in the overall protein stability remain unclear. Limited proteolysis data suggest a disordered structure for the C-terminus (residues 190−243) (*19, 24*), whereas the observation of similar α-helical content in full-length apoA-I, a (1−192) proteolytic fragment (*32*), and a truncated recombinant form (1−187) (*19*) is consistent with some helicity in the C-terminus of lipid-free apoA-I. In addition, studies of Δ(187−243) and Δ(190−243) apoA-I mutants suggest no effect of the C-terminus on the conformation and stability of the lipid-free protein (*25, 27*). However, the data of Pyle et al. (*26*) on truncated forms of apoA-I suggest an essential role of the segment (222−243) in the secondary conformation of the lipid-free protein. Thus, the secondary structure of the C-terminus of lipid-free apoA-I and its role in the maintenance of the protein integrity need to be elucidated more fully.

The focus of this study was to understand in detail the secondary structure of the C-terminal portion of lipid-free apoA-I and to probe its role in the protein conformation and stability. We produced seven apoA-I mutant forms comprising multiple point substitutions and deletions in the (165−243) portion of the protein, and analyzed the conformation and stability of the mutants by CD and fluorescence spectroscopy. Point mutations (G185P, G186P) and (L222K, F225K, F229K) were designed to probe putative loop/disordered regions. Truncations Δ(209−243), Δ(198−243), and Δ(185−243) were used to probe the role of different C-terminal segments in the protein overall structure and stability. Deletions Δ(165−175) and Δ(187−197) were designed to test our hypothesis that internal deletions of similar size may produce significantly different effects on apoA-I conformation and stability.

MATERIALS AND METHODS

C127 cells were from the American Type Culture Collection. Collagen-coated microspheres were purchased from Cellex Biosciences, Inc. Tissue culture reagents, restriction endonucleases, and other DNA modifying enzymes were purchased from Life Technologies, Inc. All other reagents were of the highest quality available.

Plasmid Constructions; Protein Expression and Purification; Sample Preparation. Construction and expression of the (L222K, F225K, F229K) substitution and the Δ(209−243) and Δ(185−243) deletion mutants were performed as described previously (*29*). The (G185P, G186P) substitution and the Δ(198−243), Δ(165−175), and Δ(187−197) deletion mutants were constructed in a similar manner. Briefly, mutants were generated by two pairs of polymerase chain reaction primers using pUCA-I_N* vector as template. The pUCA-I_N* contained a *Not*I site at the 5′ end in intron 3 and an *Xho*I site in the 3′ end of the human apoA-I gene. The first set of primers included the universal primers containing the restriction sites *Not*I (forward primer) and *Xho*I (reverse primer) flanking the apoA-I gene in the pUCA-I_N* vector. The second set included specific mutagenic primers containing the mutation of interest. Specifically, we used: (5′- A AG GAG AAC CCC CCC GCC AGA CTG -3′) and (5′- CAG TCT GGC GGG GGG GTT CTC CTT -3′) for generation of (G185P, G186P) apoA-I; (5′- GCC AAG GCC ACC TAA CAT CTG AGC ACG -3′) and (5′- CGT GCT CAG ATG TTA GGT GGC CTT GGC -3′) for Δ(198−243) apoA-I; (5′- GTG GAC GCG CTG CGC ACG CAT CTG GCC GCG CGC CTT GAG GCT CTC AAG GAG AAC -3′) and (5′- GTT CTC CTT GAG AGC CTC AAG GCG CGC GGC CAG ATG CGT GCG CAG CGC GTC CAC-3′) for Δ(165−175) apoA-I; and (5′- CTT GAG GCT CTC AAG GAG AAC GGC GGC GAG CAT CTG AGC ACG CTC AGC GAG AAG -3′) and (5′- CTT CTC GCT GAG CGT GCT CAG ATG CTC GCC GCC GTT CTC CTT GAG AGC CTC AAG -3′) for Δ(187−197) apoA-I. The DNA fragment containing the mutation of interest was digested with *Not*I and *Sal*I and cloned into corresponding sites of the pBMT3X-AI vector (*29*). The sequences of the variant apoA-I were verified by DNA sequencing.

Generation of stable mouse mammary tumor C127 cell lines expressing apoA-I, large-scale growth of cells overproducing the variant apoA-I forms, collection of the cell media containing the apoA-I forms, and purification of the proteins by ion-exchange chromatography followed by gel filtration were performed as described previously (*29*). Fractions containing greater than 95% pure apoA-I, as assessed by SDS−PAGE, were combined, dialyzed against 0.05 M ammonium bicarbonate, lyophilized, and stored at −20 °C. Plasma apoA-I was purified from isolated human plasma HDL as described (*33*); the purified protein was lyophilized and stored as described for the recombinant proteins.

For spectroscopic experiments, protein stock solutions were prepared by solubilizing the lyophilized proteins at ∼0.5 mg/mL in PBS (0.15 M NaCl, 10 mM sodium phosphate, 0.01% EDTA, and 0.02% NaN_3, pH 7.4) containing 4 M guanidine hydrochloride (GdnHCl). The protein was refolded by subsequent dialysis against GdnHCl solutions of 2.5 and 1.25 M in PBS, followed by extensive dialysis against the appropriate buffer (10 mM sodium phosphate, 0.02% NaN_3, pH 7.4, for CD experiments or PBS for fluorescence measurements). Protein solutions were used in experiments within 2−3 weeks. Protein concentration was determined by modified Lowry and BCA protein assays (Pierce, Rockford, IL). The protein concentration in samples used in CD experiments was determined before and after the experiments, and the values agreed within 10%.

Circular Dichroism Spectroscopy. CD measurements were performed on an AVIV 62DS spectropolarimeter (AVIV Associates, Inc.) equipped with a thermoelectric temperature control and calibrated with *d*-10-camphorsulfonic acid, in 2 and 1 mm path length quartz cuvettes. Protein concentrations used (25−120 μg/mL) were much lower than the critical concentration (∼0.3 mg/mL) at which plasma apoA-I self-associates under the ionic strength and pH conditions used in our experiments (*34*). Consistent with the absence of protein self-association, normalized CD spectra obtained at several protein concentrations completely superimposed for each analyzed protein. Far-UV (250−190 nm) CD spectra were recorded with a 1 nm bandwidth and 0.5−1 nm step size, at a rate of 0.05−0.1 nm/s. A total of 4−6 scans were collected and averaged, and the buffer baselines were subtracted. The spectra were normalized to the protein concentration and expressed as mean residue ellipticity, [Θ], using a mean residue weight of 115.3 for plasma and wild-type (WT) apoA-I, 115.1 for (G185P, G186P), 115.2 for (L222K, F225K, F229K), 115.0 for Δ(209−243), 117.0 for Δ(198−243), 116.4 for Δ(185−243), 114.2 for Δ(165−175), and 114.7 for Δ(187−197) apoA-I mutants. The α-helix content was estimated from the mean residue ellipticity at 222 nm, [Θ_{222}] (*35*).

Fluorescence Spectroscopy. All fluorescence experiments were carried out at 25 °C and a protein concentration of 0.06 mg/mL (at which, on the basis of our CD analysis, the proteins are monomeric). Intrinsic Trp fluorescence spectra were measured with a Hitachi F-4500 fluorescence spectrophotometer using 5 nm excitation and 2.5 nm emission slit widths, and a 295 nm excitation wavelength to avoid Tyr fluorescence. The emission was scanned from 300 to 380 nm. The wavelength of maximum fluorescence (WMF) of the Trp residues was determined from uncorrected spectra after subtraction of the buffer baseline. In fluorescence quenching experiments, spectra of proteins were recorded at increasing KI concentrations (from 0 to 0.5 M), using 5 M KI stock solution containing 1 mM sodium thiosulfate ($N_2S_2O_3$) to prevent I_3^- formation. To keep the ionic strength constant upon the additions of KI, compensatory decreasing amounts of NaCl were added from a 5 M stock solution (*36*). The integrated fluorescence intensities in the absence of the quencher and at defined KI concentrations, F_0 and F, correspondingly, were fitted to the Stern−Volmer equation:

$$F_0/(F_0 - F) = 1/f_a + 1/f_a K_{sv}[\mathrm{KI}]$$

where f_a is the fraction of Trp residues accessible to the quencher and K_{sv} is the Stern−Volmer constant that reflects the relative exposure of the quenchable residues to the quencher (*36*).

Thermal and Chemical Unfolding. Thermal unfolding was monitored by the protein ellipticity at 222 nm while heating the samples from 0 to 98 °C with a temperature step size

0.5−1 °C. To verify the equilibrium character of the thermal transitions, the melting curves were recorded for identical samples at different heating rates from 12 to 50 °C/h, with the time for recording a data point ranging from 60 to 99 s. The melting curves obtained at several protein concentrations completely superimposed, consistent with the absence of protein self-association. The midpoint (melting temperature) (T_m) and van't Hoff enthalpy (ΔH_v) of the transitions were determined by a conventional van't Hoff analysis (*37*) under assumption of the two-state unfolding model, with baselines that were obtained by linear extrapolation of the pre- and posttransitional regions. Briefly, in the transition region, at each temperature, the apparent equilibrium constant was determined as $K_{eq}(T) = (\Theta_F - \Theta_{obs})/(\Theta_{obs} - \Theta_U)$, where $\Theta_{obs}(T)$ is the observed ellipticity and $\Theta_F(T)$ and $\Theta_U(T)$ are baselines for the protein folded and unfolded states, respectively. A plot of ln K_{eq} versus $1/T$ was fitted by linear regression, and the slope and *x*-intercept provided ΔH_v and T_m values, respectively, according to the equation:

$$\ln K_{eq} = \Delta S/R - (\Delta H_v/R) \times 1/T$$

where T is temperature in degrees kelvin, $R = 1.98$ cal/(mol × K) is the universal gas constant, and ΔS is the transition entropy.

Chemical unfolding was monitored at 25 °C by the ellipticity at 222 nm and by WMF, following incubation of protein samples (0.06 mg/mL) with various concentrations of denaturant to allow proteins to reach equilibrium. Unfolding of WT and plasma apoA-I was studied using both GdnHCl (0−2.5 M) and urea (0−5 M). The unfolding of the mutant proteins was carried out either with GdnHCl or with urea. The reversibility of the chemical unfolding was verified by the CD measurements upon dilution of the protein samples containing maximal denaturant concentrations with denaturant-free buffer. The free energy difference between the native state and unfolded state of the protein in the absence of denaturant (conformational stability), $\Delta G_D°$, the midpoint of denaturation, $D_{1/2}$, and the *m* value, that reflects the steepness of the denaturation curve in the transition region, were determined using a linear extrapolation method (*38*) under the assumption of the two-state unfolding model. The linear extrapolation method, in comparison with the denaturant binding model used in other studies (*13, 16, 17*), has been shown to provide similar $\Delta G_D°$ values for both urea- and GdnHCl-induced denaturation (*39, 40*). The apparent equilibrium constant K_{eq} was determined at each denaturant concentration in the transition region as described above (for CD-monitored unfolding), or using WMF instead of Θ (for fluorescence-monitored unfolding). A plot of the Gibbs free energy, $\Delta G_D = -RT \ln K_{eq}$, where $T = 25$ °C $= 298.15$ K, versus denaturant concentration, [D], was fitted by linear regression and, after extrapolation to zero denaturant concentration, provided $\Delta G_D°$, $D_{1/2}$ (when $K_{eq} = 1$), and *m* values, according to the equation:

$$\Delta G_D = \Delta G_D° - m[D]$$

RESULTS

The purity of plasma apoA-I and recombinant WT and mutant forms of apoA-I was greater than 95%, as assessed by SDS−PAGE and Western blotting. SDS−PAGE analysis showed that the molecular weights of mutant proteins estimated from the gels were in good agreement with those predicted from the nature of the mutations (data are not shown). One liter of culture media of C127 cells yielded 0.5−3 mg of pure recombinant protein.

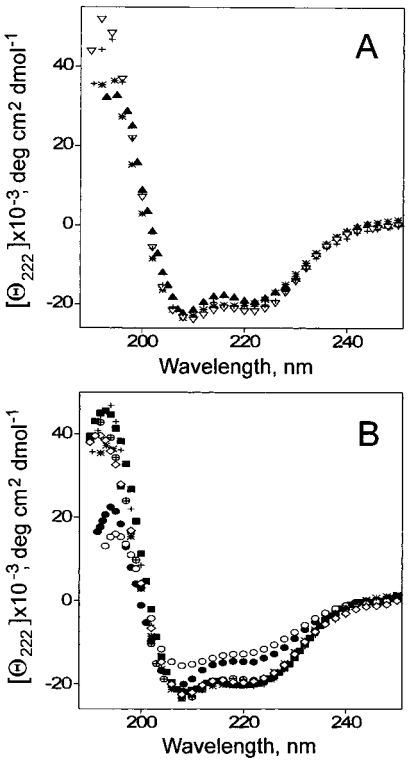

FIGURE 2: Far-UV CD spectra of plasma apoA-I (+), WT (∗), and (A) the point substitution (G185P, G186P) (▲) and (L222K, F225K, F229K) (▽) and (B) deletion Δ(209−243) (◇), Δ(198−243) (●), Δ(185−243) (■), Δ(187−197) (⊗), and Δ(165−175) (○) mutants of apoA-I at 25 °C in 10 mM sodium phosphate, 0.02% NaN_3, pH 7.4.

Far-UV CD Spectra. Figure 2 shows the far-UV CD spectra of plasma apoA-I and recombinant forms of apoA-I. The spectral value at 222 nm, [Θ_{222}], and the corresponding α-helical content are listed in Table 1. Spectra of the (G185P, G186P) substitution mutant and the Δ(209−243), Δ(185−243), and Δ(187−197) deletion mutants largely overlap with spectra of plasma apoA-I and WT at $\lambda \geq 200$ nm, suggesting similar α-helical content for these proteins. Spectral deviations at $\lambda < 200$ nm are within the noise level in the CD data that increases significantly at the short wavelengths. The triple substitution (L222K, F225K, F229K) leads to a small but significant increase in the intensity of the characteristic CD band at 222 nm (Figure 2A) that corresponds to a ∼4% increase in the α-helical content (∼10 additional helical residues) (Table 1). In contrast, the C-terminal truncation Δ(198−243) and the internal deletion Δ(165−175) lead to large spectral changes, specifically to reduced ellipticity of the CD bands at ∼222 nm and below 200 nm (Figure 2B) that corresponds to a reduction in the α-helical content by 11% (∼49 residues) for Δ(198−243) and by 20% (∼54 residues) for Δ(165−175) (Table 1).

Fluorescence Quenching. The fraction of apoA-I Trp residues accessible to the quencher I^-, f_a, and the Stern−Volmer constant, K_{sv}, that reflects a relative exposure of the quenchable residues to the quencher, are shown in Table 1. Importantly, none of the mutations studied alter the total

Table 1: Conformational Characteristics of Plasma, WT, and Variant ApoA-I[a]

apoA-I	$-[\Theta_{222}]$ at 25 °C	α-helix[b] (%)	no. of residues[c] in protein	no. of residues[c] in helix[d]	quenching by KI[e] f_a	quenching by KI[e] K_{sv} (M^{-1})
plasma	20556 ± 790	60	243	146	0.68 ± 0.05	7.1 ± 0.7
WT	19766 ± 167	58	249	144	0.64 ± 0.05	7.8 ± 0.8
(G185P, G186P)	19266 ± 500	57	249	142	0.51 ± 0.03*	8.7 ± 1.6
(L222K, F225K, F229K)	21346 ± 371**	62*	249	154 (+10)	0.72 ± 0.1	7.1 ± 1.0
Δ(209−243)	19141 ± 379	57	214 (−35)	122 (−22)		
Δ(198−243)	15187 ± 597***	47***	203 (−46)	95 (−49)	0.71 ± 0.07	11.3 ± 1.8
Δ(185−243)	20050 ± 403	59	190 (−59)	112 (−32)	0.72 ± 0.1	7.5 ± 1.1
Δ(187−197)	19318 ± 139	57	238 (−11)	136 (−8)	0.60 ± 0.02	10.2 ± 1.5
Δ(165−175)	12397 ± 659***	38***	238 (−11)	90 (−54)	0.48 ± 0.06*	12.0 ± 1.9*

[a] Values are derived from 4−8 measurements using up to 4 independent preparations of each protein. Significance of differences from the value for WT: $*p < 0.05$, $**p < 0.01$, $***p < 0.005$. WMF values for all the proteins analyzed range from 334 to 336 nm (systematic error ≤0.5 nm) and are not shown in this table. [b] Estimated from the value $[\Theta_{222}]$ at 25 °C according to (*35*); systematic error of the estimation is ±3%, statistical error is within ±1%. [c] Values in parentheses show changes in the number of residues as compared to WT. [d] Determined by multiplying the number of residues in the protein by its α-helial content. [e] Parameters of Trp fluorescence quenching: f_a, fraction of Trp residues accessible to I^-; K_{sv}, Stern−Volmer constant.

number of Trp residues in recombinant apoA-I, since all Trp residues are located in the N-terminal region (positions −3, 8, 50, 72, and 108, with position −3 in the propeptide) that is not affected by the mutations. Similar values of the quenching parameters for plasma apoA-I, WT, (L222K, F225K, F229K), Δ(209−243), Δ(185−243), Δ(198−243), and Δ(187−197) mutants indicate similar exposure of Trp in these proteins to the quencher. The double substitution (G185P, G186P) leads to a small but significant reduction in f_a, suggesting masking of one or more Trp and/or a more negatively charged environment of Trp in the mutant. The internal deletion Δ(165−175) leads to a ∼25% reduction in f_a and to more than a 50% increase in K_{sv} as compared to the values for WT, indicating substantial increase in exposure of the accessible Trp residues. Such changes suggest that the Δ(165−175) deletion disrupts the apoA-I conformation.

Thermal Unfolding. The thermal unfolding curves monitored by the ellipticity at 222 nm, $[\Theta_{222}](T)$, and the corresponding van't Hoff plots, $\ln K_{eq}(1/T)$, are shown in Figures 3 and 4, respectively. The unfolding curves recorded at several different heating rates completely superimposed, indicating the equilibrium character of the thermal transitions. Furthermore, the ellipticity at 25 °C was completely restored after heating to 70 °C followed by immediate reequilibration at 25 °C, which confirms the reversibility of the thermal unfolding. Prolonged heating to higher temperatures followed by cooling to 25 °C led to ∼10% reduction in $[\Theta_{222}]$ at 25 °C, similar to previous observations for plasma apoA-I (*18*), apolipoprotein C-I (*41*), and other proteins (*42*). Since these irreversible changes above 70 °C are relatively slow compared to the protein heat unfolding, they do not preclude equilibrium thermodynamic analysis of the unfolding transitions (*18, 41, 42*). Table 2 shows the values of the melting temperature, T_m, and the effective enthalpy, ΔH_v, determined by van't Hoff analysis. The melting curves for both point substitution mutants, (G185P, G186P) and (L222K, F225K, F229K), are slightly shifted to higher temperatures compared to those for WT (Figure 3A), in accordance with a 3 °C increase in the melting temperature T_m for both mutants (Figure 4A, Table 2) that indicates a small but significant stabilizing effect of these mutations. At 75−100 °C, the ellipticity $[\Theta_{222}]$ of the (G185P, G186P) mutant is lower than that of WT and other proteins (Figure 3A), suggesting more residual helical structure in the heat-unfolded state of this

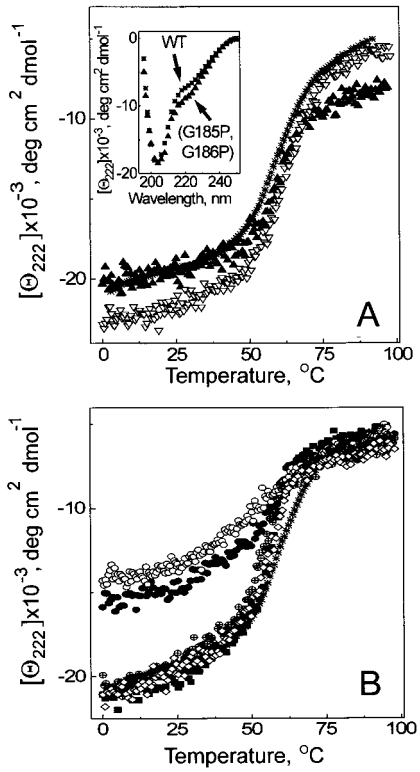

FIGURE 3: Thermal unfolding of WT (∗) and (A) the point substitution (G185P, G186P) (▲) and (L222K, F225K, F229K) (▽) and (B) deletion Δ(209−243) (◇), Δ(198−243) (●), Δ(185−243) (■), Δ(187−197) (⊗), and Δ(165−175) (○) mutants of apoA-I monitored by the ellipticity at 222 nm. The melting curve of plasma apoA-I largely overlapping with that of WT is not presented. Inset: Far-UV CD spectra of WT (∗) and the (G185P, G186P) mutant (▲) at 80 °C.

mutant. Comparison of the far-UV CD spectra of WT and (G185P, G186P) apoA-I recorded at 80 °C (Figure 3A, inset) shows similar ellipticity at 195−210 nm but significantly different ellipticity at 215−230 nm, confirming the presence of more residual helical structure in the heated−unfolded (G185P, G186P) mutant.

The melting curves for the Δ(185−243) and Δ(187−197) deletion mutants are close to that of WT (Figure 3B), and van't Hoff analysis (Figure 4B) indicates similar values of the melting temperature T_m and the effective enthalpy ΔH_v for these proteins. In contrast, the Δ(209−243), Δ(198−243),

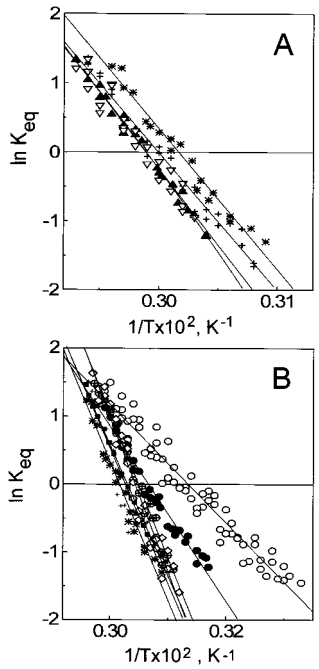

FIGURE 4: van't Hoff plots (ln K_{eq} versus $1/T$) of plasma apoA-I (+), WT (∗), and (A) the point substitution (G185P, G186P) (▲) and (L222K, F225K, F229K) (▽) and (B) deletion Δ(209−243) (◇), Δ(198−243) (●), Δ(185−243) (■), Δ(187−197) (⊗), and Δ-(165−175) (○) mutants of apoA-I.

and Δ(165−175) mutations lead, respectively, to a 3, 5, and 13 °C decrease in T_m (Table 2), indicating the destabilizing effect of these three deletions, with the most significant effect being for the Δ(165−175) internal deletion. In addition, the shapes of the melting curves for the Δ(198−243) and Δ-(165−175) mutants suggest lower cooperativity of the thermal transitions (Figure 3B). van't Hoff analysis (Figure 4B) indicates a 13 and 26 kcal/mol reduction in the effective enthalpy ΔH_v for the Δ(198−243) and Δ(165−175) mutants, respectively, that is a significant reduction compared to the $\Delta H_v = 41 \pm 1$ kcal/mol for WT.

Denaturant-Induced Unfolding. Chemical unfolding curves of the proteins monitored by CD and fluorescence spectroscopy are shown in Figures 5 and 6, respectively. The conformational stability $\Delta G_D°$, midpoint of denaturation $D_{1/2}$, and *m* values derived from these data are shown in Table 2. $D_{1/2}$ and *m* values are presented for GdnHCl-induced unfolding. $\Delta G_D°$ values are presented for both GdnHCl- and urea-induced unfolding. $\Delta G_D°$ values determined from GdnHCl- and urea-induced unfolding were identical.

The (G185P, G186P) mutation leads to a 0.4 kcal/mol increase in $\Delta G_D°$ (Table 2) indicating a small but significant stabilizing effect of the double Pro substitution. At GdnHCl concentrations ≥2 M, the values of $[\Theta_{222}]$ and WMF for (G185P, G186P) apoA-I are lower than those for WT (Figures 5A and 6A), suggesting more residual helical structure in the chemically unfolded state of this mutant, similar to the thermally unfolded state of the same mutant. The (L222K, F225K, F229K) mutation leads to a small but statistically significant increase in the midpoint of the urea-induced denaturation (2.5 ± 0.1 vs 2.2 ± 0.1 M for WT, $p < 0.05$, not shown in Table 2), suggesting a small stabilizing effect of the triple point mutation.

The unfolding curves and values of $\Delta G_D°$, *m*, and $D_{1/2}$ for the Δ(185−243) and Δ(187−197) mutants are close to those of WT, suggesting that these two mutations do not affect the protein chemical stability or unfolding cooperativity. The C-terminal truncation Δ(209−243) leads to a 0.5 kcal/mol reduction in $\Delta G_D°$ (Table 2) and a 0.5 M reduction in the midpoint of the urea-induced denaturation. The larger C-terminal truncation, Δ(198−243), leads to a 0.5 kcal/mol reduction in $\Delta G_D°$ and to a 0.2 M reduction in $D_{1/2}$ (Table 2). This indicates that C-terminal truncations through residues 209 or 198 destabilize apoA-I. The internal deletion Δ(165−175) leads to the largest changes in the denaturant-unfolding curves of apoA-I (Figure 5C and 6B). The shape of the denaturation curve for this mutant indicates low cooperativity. The very low α-helix content and the absence of a plateau at low denaturant concentrations indicate that even in the absence of denaturant the mutant is destabilized. This is consistent with the large reductions in $\Delta G_D°$ (1.4 ± 0.1 vs 2.3 ± 0.1 kcal/mol for WT), the *m* value, and the midpoint of denaturation $D_{1/2}$ (0.7 ± 0.09 vs 1.1 ± 0.06 M for WT). These data indicate a large destabilizing effect of the internal deletion Δ(165−175) on the apoA-I secondary structure.

In all the experiments, all the parameters characterizing the conformation and stability of WT do not differ significantly from the corresponding parameters for plasma apoA-I (Tables 1 and 2). This indicates that the six-residue propeptide in the recombinant proteins does not contribute significantly to their secondary structure and stability.

DISCUSSION

In this study, we probed specific regions of the C-terminus (residues 165−243) of apoA-I, by deletion or substitution mutations, to determine their role in the overall structure and stability of the lipid-free protein. The results of the study provide further understanding of the molecular details of apoA-I secondary structure in solution and appear consistent with the presence of stable helical structure in the C-terminus.

The double substitution of Pro for Gly185, Gly186 was designed to test whether the mutated residues are located in a helical or disordered/loop region. Pro substitutions in the middle of protein α-helices are known to disrupt and destabilize the protein secondary structure (*43*, *44*). In contrast, Pro substitutions in loop/disordered regions do not disrupt the protein structure and may lead to entropic stabilization by restricting the configurational entropy of the unfolded state (*45*). In lipid-free apoA-I, the (G185P, G186P) double substitution does not change the α-helical content and leads to an increase in the protein stability. These results strongly suggest a loop/disordered region location of G185 and G186 consistent with the predicted location of these residues in the model of Nolte and Atkinson (*23*) (Figure 1A) and inconsistent with the helix location of the residues in the structure proposed by Roberts et al. (*24*) (Figure 1B). The presence of more residual helical structure in the thermally or chemically unfolded state of the (G185P, G186P) mutant (Figures 3A, 5A, 6A, and 3A inset) may result from the restrictive effect of Pro on the unfolded conformation of lipid-free apoA-I. Fluorescence analysis shows that the (G185P, G186P) mutation leads to reduction in the fraction of Trp residues accessible to the negatively charged quencher. This effect of the double mutation located in the C-terminal part of apoA-I on the exposure of Trp residues located exclusively in the N-terminal half of the

Table 2: Thermodynamic Parameters of Plasma, WT, and Variant ApoA-I[a]

apoA-I	T_m[b] (°C)	ΔH_v[b] (kcal/mol)	$\Delta G_D°$[c] (kcal/mol)	m[c] [kcal (mol of apoA-I)$^{-1}$ (mol of GdnHCl)$^{-1}$]	$D_{1/2}$[c] (M)
plasma	59 ± 2	40 ± 1.6	2.4 ± 0.1	2.2 ± 0.1	1.1 ± 0.05
WT	58 ± 1	41 ± 1	2.3 ± 0.1	2.1 ± 0.15	1.1 ± 0.06
(G185P, G186P)	61 ± 1*	44 ± 3	2.7 ± 0.1*	2.4 ± 0.1	1.2 ± 0.05
(L222K, F225K, F229K)	61 ± 1*	44 ± 1	2.5 ± 0.1		
Δ(209−243)	55 ± 1*	45 ± 2	1.8 ± 0.2*		
Δ(198−243)	53 ± 1**	28 ± 3***	1.8 ± 0.1*	2.0 ± 0.1	0.9 ± 0.05*
Δ (185−243)	57 ± 1	39 ± 0.4	2.2 ± 0.1	2.0 ± 0.15	1.1 ± 0.1
Δ(187−197)	56 ± 2	43 ± 2	2.3 ± 0.2	2.3 ± 0.3	1.0 ± 0.07
Δ(165−175)	45 ± 1***	15 ± 3***	1.4 ± 0.1***	1.8 ± 0.1*	0.7 ± 0.09**

[a] Values are the average ± standard deviation from 3−10 experiments for 2−4 independent preparations of each protein. Significance of differences from the value for WT: $*p < 0.05$, $**p < 0.01$, $***p < 0.005$. [b] Melting temperature (T_m) and effective enthalpy (ΔH_v) of thermal unfolding were determined from van't Hoff analysis of the melting curves monitored by ellipticity at 222 nm. [c] Conformational stability, $\Delta G_D°$, midpoint of chemical denaturation, $D_{1/2}$, and m values were determined by the linear extrapolation method from CD-monitored and, for most of the proteins, from fluorescence-monitored unfolding curves and averaged. GdnHCl-induced unfolding was monitored by both CD and fluorescence; urea-induced unfolding was monitored by CD only. $\Delta G_D°$ values were determined from both GdnHCl- and urea-induced unfolding for WT and plasma apoA-I, from GdnHCl-induced unfolding for (G186P, G186P), Δ(198−243), Δ(185−243), Δ(187−197), and Δ(165−175) apoA-I, and from urea-induced unfolding for (L222K, F225K, F229K) and Δ(209−243) apoA-I. $D_{1/2}$ and m values in the table are shown for GdnHCl-induced unfolding; these values are not presented for (L222K, F225K, F229K) and Δ(209−243) apoA-I, since urea was used for unfolding of these two mutants.

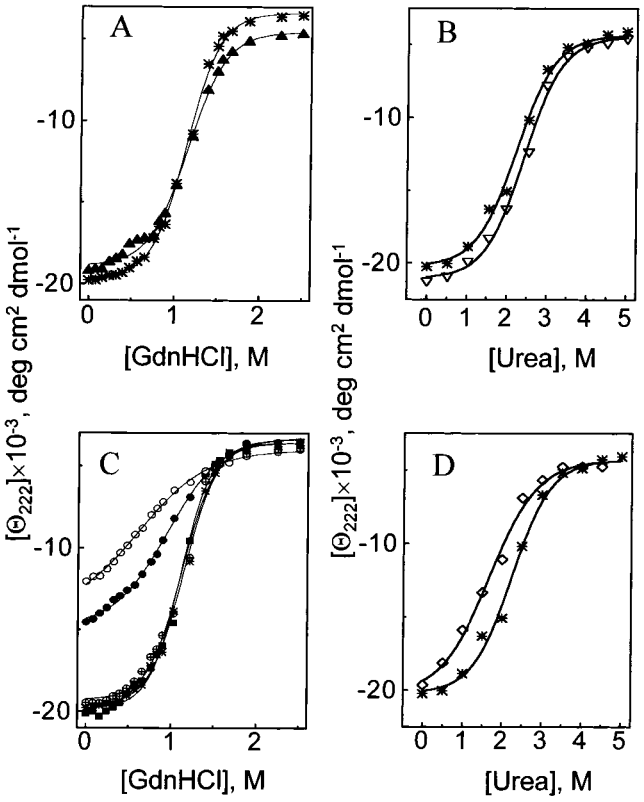

FIGURE 5: Denaturant-induced unfolding monitored by ellipticity at 222 nm. (A) The (G185P, G186P) point substitution (▲), (B) the (L222K, F225K, F229K) point substitution (▽), (C) the deletion mutants Δ(198−243) (●), Δ(185−243) (■), Δ(187−197) (⊗), and Δ(165−175) (○), and (D) the deletion mutant Δ(209−243) (◇). Panels A and C present GdnHCl-induced denaturation; panels B and D present urea-induced denaturation; WT (∗) is shown for comparison in each panel.

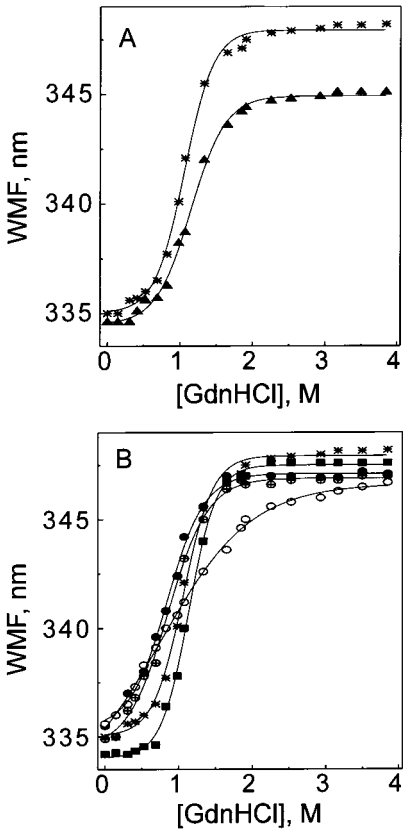

FIGURE 6: GdnHCl-induced unfolding monitored by WMF using 295 nm excitation wavelength. (A) The (G185P, G186P) point substitution (▲) and (B) the deletion mutants Δ(198−243) (●), Δ(185−243) (■), Δ(187−197) (⊗), and Δ(165−175) (○). WT (∗) is shown for comparison in each panel.

molecule suggests a tertiary structure of lipid-free apoA-I in which the C-terminal region is close to the N-terminal region. Recent observations of Tricerri et al. on two cysteine mutants of apoA-I lead to a similar suggestion [unpublished data, reviewed in (*46*)].

The triple substitution of charged for large hydrophobic groups, (L222K, F225K, F229K), was designed to probe the position of the mutated residues in the tertiary structure of lipid-free apoA-I. If the mutated residues were buried, as is typical for large hydrophobic groups in globular proteins, substitution of these residues to charged groups would be strongly destabilizing (*47, 48*). However, our CD analysis shows a small increase in the α-helical content and stability resulting from the (L222K, F225K, F229K) mutation. This suggests that L222, F225, and F229 are not involved in hydrophobic stabilizing interactions in lipid-free apoA-I and are probably solvent exposed. This agrees with the predicted positions for L222, F225, and F229 in a loop/disordered

region (Figure 1A,B), with the exception of L222 that is predicted to be located at the end of the long penultimate helix in model A. However, Pro in position 220 of the apoA-I sequence is also consistent with the loop/disordered region comprising the entire 11-mer "A" unit 220−230 (including L222) in the lipid-free protein. The crystal structure of Δ-(1−43) apoA-I also shows a loop encompassing this region (*20*). The CD analysis shows that the (L222K, F225K, F229K) mutation results in a ∼10 residue increase in the number of helical residues, suggesting that the loop/disordered region (residues 220−230) may form a helix in the mutant protein. Thus, our results on two substitution mutants suggest the presence in the apoA-I C-terminus of two loop/disordered regions comprising residues G185, G186 and residues L222, F225, F229, respectively.

To probe the secondary structure between these two putative loop/disordered regions, we studied three C-terminal truncations, Δ(209−243), Δ(198−243), and Δ(185−243), and the 11-mer internal deletion, Δ(187−197). The Δ(209−243) truncation does not affect the protein α-helical content and destabilizes the protein, suggesting that the segment 209−243 is involved in stabilizing interactions in native lipid-free apoA-I. The larger truncation, Δ(185−243), and the internal deletion Δ(187−197) do not have any significant effect on the apoA-I overall conformation, stability, or unfolding cooperativity. The intermediate C-terminal truncation, Δ(198−243), surprisingly, leads to a large reduction in the apoA-I α-helical content, stability, and unfolding cooperativity. These results appear to be in agreement with the presence of stable helical structure in the C-terminus, as proposed in model A, rather than with a disordered C-terminus, as proposed in model B (Figure 1).

According to our CD analysis, the 35-residue deletion Δ-(209−243) results in a ∼22-residue reduction in the number of helical residues. This number is very close to the number of deleted helical residues in the structure shown in Figure 1A: the mutation deletes the 12-residue C-terminal helix (residues 231−242) and the 11-mer "A" unit (residues 209−219) of the putative long penultimate helix, and thus removes 23 helical residues. The deleted segment 220−230 has been suggested to form a loop/disordered region, from our analysis of the (L222K, F225K, F229K) mutation. The secondary conformation of the truncated protein (1−208) remains similar to native apoA-I, consistent with the data obtained. In model B, no helical residues are deleted by the Δ(209−243) truncation, implying, in the context of our CD analysis, an indirect effect of the mutation, namely, unfolding of a ∼22-residue helical segment in the remaining helical structure (region 8−189). However, in view of the molten globular-like state of lipid-free apoA-I in which α-helices are only weakly stabilized by tertiary interactions (*9, 18, 19*), indirect effects of mutations seem less likely than local, direct effects.

The internal deletion Δ(187−197) results in a reduction in the number of helical residues by ∼8 (Table 1) that is similar to the number of deleted residues, 11. This suggests a mostly helical structure of the deleted segment 187−197 that is consistent with model A. In model B that predicts mostly disordered structure for segment 187−197, our analysis, again, implies indirect effect of the mutation, such as unfolding of a helical segment in the remaining protein. Thus, our studies of the Δ(209−243) and Δ(187−197) mutants are consistent with the helical structure of segments 231−242, 209−219, and 187−197, in agreement with the secondary structure predicted for region 187−243 by model A (Figure 1). In the context of these two mutants, the segment 198−208 may have helical and/or disordered structure. However, our analysis of Δ(198−243) truncation seems inconsistent with the disordered structure of the segment 198−208.

As demonstrated by studies of large internal deletions of apoA-I (*31*) and a C-terminal truncation through residue 187 (*19, 27*), deletions made through loop/disordered regions do not result in major changes in the secondary structure of apoA-I. The Δ(198−243) mutation has a significant disrupting and destabilizing effect on apoA-I secondary structure, suggesting that this truncation is made through a helical region. Moreover, the helical structure of segment 198−208, and thus, the whole segment 187−219, in agreement with model A (Figure 1), reasonably explains the experimental data on the α-helical content and stability of the Δ(198−243) mutant. From our CD analysis, the 46-residue deletion Δ(198−243) results in an ∼49-residue reduction in the number of helical residues. In model A, this deletion removes the 12-residue C-terminal helix and the helical structure between residues 198 and 219, leaving the single helical "B" repeat (residues 187−197) that corresponds to the removal of 34 helical residues. In contrast to reduction in the length of the putative extended helical region 187−219 by a single 11-mer repeat, as in the Δ(209−243) or Δ(187−197) mutations, significant truncation of this region to a single 11-mer unit in the Δ(198−243) mutation may result in destabilization of the remaining unit. Unfolding of this remaining unit, 187−197, may account for loss of an additional 11 helical residues that results in a 45-residue total reduction in the number of helical residues following the Δ(198−243) truncation. This is similar to the observed experimental value of ∼49 residues. Moreover, unfolding of the unit 187−197 may alter intramolecular interactions, leading to the observed reduction in protein stability and unfolding cooperativity. In model B, the disordered structure of the C-terminus implies, again, that some other segments of 49-residue total length unfold in the remaining helical structure following the Δ(198−243) deletion. Such a large reduction in the helical content of the remaining protein is unlikely to result in no significant effect of the Δ(198−243) deletion on the tryptophan exposure observed in the fluorescence quenching experiments. Thus, overall, our studies of the Δ(209−243), Δ(187−197), and Δ(198−243) deletions are consistent with the extended helical structure of the region 187−219.

The large, 59-residue C-terminal truncation, Δ(185−243), does not affect apoA-I α-helical content, tryptophan exposure, stability, and unfolding cooperativity. This is in a good agreement with data from the groups of Brouilette and Jonas that have shown that C-terminal truncations through residues 187 (*19, 27*) and 190 (*25*) have no significant effect on apoA-I conformation and stability. The Δ(185−243) deletion results in a loss of ∼32 helical residues (Table 1). Assuming the existence of the short C-terminal helix and the extended helical region 187−219, in accordance with the analysis of both point mutations and deletions Δ(209−243), Δ(187−197), and Δ(198−243), and the predicted secondary structure (Figure 1A), the Δ(185−243) deletion removes both the short

C-terminal helix and the entire extended helical region 187−219 that corresponds to 45 residues of helical structure. The ∼13-residue difference representing an increase in helical structure in the remaining protein may be explained by folding of an additional segment triggered by the Δ(185−243) truncation. This relatively small folding (only ∼13 residues) may be consistent with the observed fluorescence quenching parameters, stability, and unfolding cooperativity that are unaffected by the Δ(185−243) truncation. Our experimental data do not provide any direct evidence on the location of a segment that may fold in the Δ(185−243) mutant. One candidate for this folding may be the segment 44−60 that is folded in the crystal structure of Δ(1−43) apoA-I (*20*); another candidate for this folding may be one of the central helices shown in Figure 1A, that may be unfolded in native lipid-free apoA-I, as will be suggested below. Additional experiments are required to test these hypotheses. According to Rogers et al. (*19*), the Δ(187−243) truncation resulted in a loss of ∼38 helical residues that is similar to the ∼32-helical residue loss in the Δ(185−243) truncation analyzed in our study. Interpretation of these data by Rogers et al. (*19*) in the context of model B accounts for the loss of the 38 helical residues solely by unfolding of helices in the remaining protein. Again, such a large unfolding of helical structure in the region 8−186 (Figure 1B) is unlikely to result in no changes in fluorescence quenching parameters, stability, and unfolding cooperativity, which is the case for both truncations Δ(187−243) (*19*) and Δ(185−243) (Tables 1 and 2).

Our results on the internal deletion Δ(187−197) and the large C-terminal deletion Δ(185−243), that have no significant effect on the overall apoA-I conformation and stability, are consistent with the molten globule state of the protein in solution, in accord with earlier studies of apoA-I (*9, 18, 19*). However, the significant alterations in the protein stability caused by the Δ(198−243) deletion, as well as the effect of the (G185P, G186P) mutation on tryptophan exposure, suggest that some tertiary interactions do contribute to the structure and stability of lipid-free apoA-I. The reduction in protein stability observed for the Δ(209−243) mutation could also result from the loss of stabilizing interactions that may exist between the short C-terminal helix and the extended helical region 187−219 in lipid-free apoA-I. This suggestion is consistent with the unaffected stability of the Δ(187−197) and Δ(185−243) mutants. The Δ(187−197) mutant does not remove the short C-terminal helix, and the Δ(185−243) mutant removes both the short C-terminal helix and the entire helical region 187−219. Unaffected stability of the Δ(185−243) mutant suggests no stabilizing interactions of the extended helical region 187−219 and the short C-terminal helix with the rest of the protein (residues 1−184). This is consistent with a suggestion of Rogers et al. (*19*), that the C-terminus of apoA-I (residues 187−243) does not play a major role in apoA-I stability. However, the destabilizing effects of the Δ(209−243) and Δ(198−243) deletions unambiguously show that smaller constituents of the apoA-I C-terminus, fragments 198−243 and 209−243, are important for protein stability.

Thus, overall, our experimental data on the mutations of the C-terminus 185−243 appear consistent with the secondary structure predicted for this region by Nolte and Atkinson (*23*) (Figure 1A). The predicted conformation was based on the apoA-I sequence and, therefore, reflects the propensity of the sequence to fold into a particular secondary structure. However, the model was constrained by using the CD data for lipid-bound apoA-I and should contain more helical segments(s) compared to a secondary structure prediction that would use CD data for the lipid-free protein for quantitation. Indeed, model A predicts 168 helical residues (*23*), compared to ∼146 helical residues determined from the CD analysis of lipid-free plasma apoA-I (Table 1). Significantly, the ∼22-residue difference corresponds to the number of residues in any of the predicted 22-residue tandem repeats that may form helices. This is consistent with a secondary structure of lipid-free apoA-I that differs from the predicted secondary structure of lipid-bound protein (Figure 1A) by unfolding of one helical segment. Observations of Davidson et al. (*25*) suggest that a segment in the portion 139−243 of apoA-I forms additional α-helical structure when apoA-I binds lipids. One of the central 20-residue helices predicted by model A (Figure 1) may be unfolded in the lipid-free state. Folding of this repeat (or a part of it) may be triggered by the Δ(185−243) truncation. Our ongoing studies on probing the structure of central regions of apoA-I may provide new information on potential segments that are unfolded in the lipid-free state.

Compared to the other mutations, the internal deletion Δ(165−175) reduces the apoA-I α-helical content, stability, and unfolding cooperativity, and alters tryptophan exposure most dramatically. This 11-mer deletion leads to reduction in the number of helical residues by ∼54, indicating unfolding of at least 43 helical residues in the remaining protein. The Δ(165−175) deletion corresponds to removing a complete 11-mer "A" unit that comprises a part of helix 7 and the loop preceding it in model A (Figure 1). This deletion results in the juxtaposition of two 11-mer "B" repeats (residues 154−164 and 176−186) and ultimately may lead to juxtaposition of three 11-mer repeats, "A", "B", and "B", comprising residues 145−164 and 176−186. In the mutant, this 33-residue segment is connected by the loop comprising residues G185 and G186 to the extended helical region 187−219 consisting of three other combined 11-mer repeats, "B", "B", and "A" (Figure 1A). Thus, the Δ(165−175) deletion probably completely rearranges the central region between residues 145 and 183 that, in turn, significantly alters intramolecular interactions precluding proper apoA-I folding.

The studies of the Δ(165−175) internal deletion indicate that the presence of segment 165−175 is critical for proper apoA-I folding and demonstrate the importance of the correct juxtaposition of helical segments in the central region for proper protein folding. Interestingly, a naturally occurring apoA-I mutation (P165R) that affects the critical (165−175) unit has been shown to cause a large reduction in the ability of apoA-I to promote cholesterol efflux and to activate LCAT and is associated with low HDL-cholesterol level in heterozygous carriers (*49*). One other 11-mer internal deletion of apoA-I, Δ(88−98), has been shown recently (*27*) to reduce dramatically the protein α-helical content and stability. Thus, two 11-mer internal deletions, Δ(88−98) and Δ(165−175), preclude the proper apoA-I folding and destabilize the protein, whereas the third one, Δ(187−197), does not. This reflects the complexity and variety of interresidue and interfragment interactions that are critical for maintaining apoA-I integrity.

Overall, the current study provides new insights into the structure and stability of apoA-I in the lipid-free state that are important for understanding the functions of this important protein. Consistent with recent fluorescence studies of mutant forms of apoA-I that suggest an organization of the N-terminal half of lipid-free apoA-I into a bundle of helices (*50*), and with our fluorescence quenching data for the (G185P, G186P) mutant, apoA-I in solution may form a bundle of helices, similar to that proposed by model B, but with helical structure of the C-terminus, as proposed by model A (Figure 1). Our ongoing studies designed to probe the structure of the N-terminal and central parts of apoA-I by mutation are expected to provide additional information that will help to propose a more detailed model of lipid-free apoA-I conformation.

ACKNOWLEDGMENT

We thank Gayle Forbes for expert technical assistance with tissue culture procedures, Cheryl England for purification of plasma apoA-I, and Dr. Theresa Davies from the Department of Biochemistry of the Boston University School of Medicine for providing the possibility of using the fluorescence spectrometer.

REFERENCES

1. Fielding, C. J., and Fielding, P. E. (1995) *J. Lipid Res. 36*, 211−228.
2. Breslow, J. L. (1993) *Proc. Natl. Acad. Sci. U.S.A. 90*, 8314−8318.
3. Pastzy, C., Maeda, N., Verstuyft, J., and Rubin, E. M. (1994) *J. Clin. Invest. 94*, 899−903.
4. Jonas, A. (1991) *Biochim. Biophys. Acta 108*, 205−220.
5. Meng, Q.-H., Bergeron, J., Sparks, D. L., and Marcel, Y. L. (1995) *J. Biol. Chem. 270*, 8588−8596.
6. Hammad, S. M., Stefansson, S., Twal, W. O., Drake, C. J., Fleming, P., Remaley, A., Brewer, H. B., and Argraves, W. S. (1999) *Proc. Natl. Acad. Sci. U.S.A. 96*, 10158−10163.
7. Mendez, A. J. (1997) *J. Lipid Res. 38*, 1807−1821.
8. Rothblat, G. H., de la Llera-Moya, M., Atger, V., Kellner-Weibel, G., Williams, D. L., and Phillips, M. C. (1999) *J. Lipid Res. 40*, 781−796.
9. Segrest, J. P., Jones, M. K., De Loof, H., Brouillette C. G., Venkatachalapathi, Y. V., and Anantharamaiah, G. M. (1992) *J. Lipid Res. 33*, 141−166.
10. Sparks, D. L., Anantharamaiah, G. M., Segrest, J. P., and Phillips, M. C. (1995) *J. Biol. Chem. 270*, 5151−5157.
11. Sorci-Thomas, M. G., Curtiss, L., Parks, J. S., Thomas, M. J., and Kearns, M. W. (1997) *J. Biol. Chem. 272*, 7278−7284.
12. Sorci-Thomas, M. G., Currtiss, L., Parks, J. S., Thomas, M. J., Kearns, M. W., and Landrum, M. (1998) *J. Biol. Chem. 273*, 11776−11782.
13. Parks, J. S., and Gebre A. K. (1997) *J. Lipid Res. 38*, 266−275.
14. Burgess, J. W., Frank, P. G., Franklin, V., Liang, P., McManus, D. C., Desforges, M., Rassart, E., and Marcel, Y. L. (1999) *Biochemistry 38*, 14524−14533.
15. Braschi, S., Neville, T. A.-M., Vohl, M.-C., and Sparks, D. L. (1999) *J. Lipid Res. 40*, 522−532.
16. Sparks, D. L., Lund-Katz, S., and Phillips, M. (1992) *J. Biol. Chem. 267*, 25839−25847.
17. Sparks, D. L., Lund-Katz, S., Davidson, W. S., and Phillips, M. (1995) *J. Biol. Chem. 270*, 26910−26917.
18. Gursky, O., and Atkinson, D. (1996) *Proc. Natl. Acad. Sci. U.S.A. 93*, 2991−2995.
19. Rogers, D. P., Roberts, L. M., Lebowitz, J., Engler, J. A., and Brouilette, C. G. (1998) *Biochemistry 37*, 945−955.
20. Borhani, D. W., Rogers, D. P., Engler, J. A., and Brouilette, C. G. (1997) *Proc. Natl. Acad. Sci. U.S.A. 94*, 12191−12296.
21. Rogers, D. P., Brouilette, C. G., Engler, J. A., Tendian, S. W., Roberts, L., Mirsha, V., Anantharamaiah, G. M., Lund-Kutz, S., Phillips, M. C., and Ray, M. J. (1997) *Biochemistry 36*, 288−300.
22. Brouilette, C. G., and Anantharamaiah, G. M. (1995) *Biochim. Biophys. Acta 1256*, 103−129.
23. Nolte, R. T., and Atkinson, D. (1992) *Biophys. J. 63*, 1221−1239.
24. Roberts, L. M., Ray, M. J., Shih, T.-W., Hayden, E. H., Reader, M. M., and Brouillette, C. G. (1997) *Biochemistry 36*, 7615−7624.
25. Davidson, W. S., Hazlett, T., Mantulin, W. W., and Jonas, A. (1996) *Proc. Natl. Acad. Sci. U.S.A. 93*, 13605−13610.
26. Pyle, L., Sawyer, W. H., Fujiwara, Y., Mitchell, A., and Fidge, N. H. (1996) *Biochemistry 35*, 12046−12052.
27. Rogers, D., Roberts, L. M., Lebowitz, J., Datta, G., Anantharamaiah, G. M., Engler, J., and Brouilette, C. G. (1998) *Biochemistry 37*, 11714−11725.
28. Holvoet, P., Zhao, Z., Vanloo, B., Vos, R., Derridder, E., Dhoest, A., Taveirne, J., Brouwers, E., Demarsin, E., Engelborghs, Y., Rosseneu, M., Collen, D., and Brasseur, R. (1995) *Biochemistry 34*, 13334−13342.
29. Laccotripe, M., Makrides, S. C., Jonas, A., and Zannis, V. I. (1997) *J. Biol. Chem. 272*, 17511−17522.
30. Lindholm, E. M., Bielicki, J. K., Curtiss, L. K., Rubin, E. M., and Forte, T. M. (1998) *Biochemistry 37*, 4863−4868.
31. Frank, P. G., Bergeron, J., Emmanuel, F., Lavigne, J.-P., Sparks, D. L., Denefle, P., Rassart, E., and Marcel, Y. L. (1997) *Biochemistry 36*, 1798−1806.
32. Ji, Y., and Jonas, A. (1995) *J. Biol. Chem. 270*, 11290−11297.
33. Wetterau, J. R., and Jonas, A. (1982) *J. Biol. Chem. 257*, 10961−10966.
34. Donovan, J. M., Benedek, G. B., and Carey, M. C. (1987) *Biochemistry 26*, 8116−8125.
35. Chen, Y.-H., Yang, J. T., and Martinez, H. M. (1972) *Biochemistry 11*, 1420−1431.
36. Lehrer, S. S. (1971) *Biochemistry 10*, 3254−3263.
37. Pace, C. N., Shirley, B. A., and Thomson, J. A. (1989) in *Protein Structure* (Creigton, T. E., Ed.) pp 311−330, IRL Press, Cary, NC.
38. Pace, C. N., and Vanderburg, K. E. (1979) *Biochemistry 18*, 288−292.
39. Pace, C. N. (1986) *Methods Enzymol. 131*, 266−280.
40. Santoro, M. M., and Bolen, D. W. (1988) *Biochemistry 27*, 8063−8068.
41. Gursky, O., and Atkinson, D. (1998) *Biochemistry 37*, 1283−1291
42. Carra, J. H, Anderson, E. A., and Privalov, P. L. (1994) *Protein Sci. 3*, 944−951.
43. O'Nell, K. T., and De Grado, W. F. (1990) *Science 250*, 646−651.
44. Shulman, B. A., and Kim, P. S. (1996) *Nat. Struct. Biol. 3*, 682−687.
45. Shortle, D. (1989) *J. Biol. Chem. 264*, 5315−5318.
46. Frank, G. P., and Marcel, Y. L. (2000) *J. Lipid Res. 41*, 853−872.
47. Shortle, D., Stites, W. E., and Meeker, A. K. (1990) *Biochemistry 29*, 8033−8041.
48. Gromiha, M. M., Oobatake, M., Kono H., Uedaira, H., and Sarai, A. (1999) *Protein Eng. 12*, 549−555.
49. Daum, U., Leren, T. P., Langer, C., Chirazi, A., Cullen, P., Pritchard, P. H., Assmann, G., and von Eckardstein, A. (1999) *J. Lipid Res. 40*, 486−494.
50. Davidson, W. S., Arnvig-McGuire, K., Kennedy, A., Kosman, J., Hazlett, T. L., and Jonas, A. (1999) *Biochemistry 38*, 14387−14395.

BI0014406